ef500251h

DATASET · JUNE 2014

READS
19

7 AUTHORS, INCLUDING:

He Boshu
Beijing Jiaotong University
52 PUBLICATIONS **249** CITATIONS
SEE PROFILE

Zhipeng Duan
Beijing Jiaotong University
42 PUBLICATIONS **347** CITATIONS
SEE PROFILE

energy&fuels

Article

pubs.acs.org/EF

Pressurized Thermogravimetric Study on the Hydropyrolysis and Hydrogasification Kinetics of a Bituminous Coal

Linbo Yan,[†] Boshu He,*[,†] Tianyi Hao,[‡] Xiaohui Pei,[†] Xusheng Li,[†] Chaojun Wang,[†] and Zhipeng Duan[†]

[†]Institute of Combustion and Thermal System, School of Mechanical, Electronic and Control Engineering, Beijing Jiaotong University, Beijing 100044, People's Republic of China

[‡]Department of Thermal Engineering, Key Laboratory for Thermal Science and Power Engineering of Ministry of Education, Tsinghua University, Beijing 100084, People's Republic of China

ABSTRACT: Coal hydropyrolysis (CHP) and coal hydrogasification (CHG) are two important processes during coal conversion in a hydrogen atmosphere. Much attention has been paid on this clean coal conversion technology because of its advantages. In this work, the CHP and CHG kinetic characteristics of a bituminous coal are studied in a pressurized thermogravimetric analyzer (P-TGA). The effects of the pressure on the CHP and CHG kinetics of the bituminous coal are detected with the non-isothermal thermogravimetric method. In addition, the kinetic compensation effect (KCE) and isokinetic points of the two processes are investigated. Besides, the kinetic triplets, including the pre-exponent factor, the activation energy and mechanism function are also calculated and defined for all of the cases during the CHP and CHG processes. Meaningful and interesting conclusions are finally obtained from this study. The initial pyrolysis temperature will increase with the reaction pressure when the pressure is within 3 MPa. The appearing time of the weight loss peak rate will be delayed when the pressure is lower than 2 MPa, and then it will become earlier gradually with the pressure increment. The weight loss peak rate will decrease sharply when the pressure is increased from 0.1 to 1 MPa, and then it will increase gradually with the reaction pressure increment. The KCE phenomenon during the CHP process is not detected, and the isokinetic point is not found. The KCE can be detected during the CHG process when the reaction pressure is within 3 MPa and the isokinetic point temperature is found as 1041.0 K.

1. INTRODUCTION

Coal hydrogasification (CHG) is a very promising technology for clean and efficient coal utilization.[1−4] It has attracted more and more attention recently for its obvious advantages. For example, the hydrogasification reaction is exothermic, and thus, no additional heat is required. The direct product of hydrogasification is methane; therefore, no additional methanator is required. The hydrogasification process has high thermal efficiency, close to 80%, and there is no requirement for a catalyst.[1] Many researchers from all over the world have contributed to the development of CHG, and the kinetic characteristics were also studied. Some lab-scale experiments[5−7] had been implemented to study the effects of different operating conditions on the CHG products. Some semi-industry devices[8−10] had also been built, and the corresponding CHG experimental reports had been published to help researchers develop their corresponding kinetic mechanisms. As the primary process of the CHG, coal hydropyrolysis (CHP) also plays a very important role during the whole reaction process. In addition, CHP itself is also a promising coal conversion technology for clean coal utilization, and many researchers had performed a lot of work on the CHP process.[11,12] During the last few decades, a lot of studies on CHG technology have been performed. However, most of those studies were performed in the fixed-bed gasifiers, and a few were performed in the entrained flow-bed gasifiers. In these two types of gasifiers, the effects of the reaction conditions on the yields of the hydropyrolysis and hydrogasification processes can be investigated and the general kinetic process can be detected. The detailed kinetic processes, however, cannot be found from those experiments. To find out the detailed kinetic process, thermogravimetric analyses on CHP and CHG should be performed. However, because of the strict requirements on the experiment equipment and the safety of these experiments, reports on the CHP and CHG kinetics by thermogravimetric analyses are still rarely found, which is adverse to the further development of the CHG and CHP technologies.

In this work, both the CHG and CHP kinetic characteristics of a bituminous coal are studied in a pressurized thermogravimetric analyzer (P-TGA). The effect of hydrogen pressure is detected, and the thermogravimetric (TG) and derivative thermogravimetric (DTG) curves obtained at different pressures are compared and analyzed. On the basis of the TG and DTG curves, the kinetic triplets of the CHG and CHP processes are defined. In addition, the kinetic compensation effect (KCE) during the CHP and CHG processes is studied, and the isokinetic points of the two processes are investigated.

2. EXPERIMENTAL SECTION

The experiments in this work were implemented in a P-TGA called TherMax 500 made by the Thermo Fisher Scientific Corporation. The whole experiment system includes a suspension pressurized balance, a furnace, an elevator, a control panel, a holder, several gas vessels, and a supervisory control computer running the Cahn Thermal Analysis software. As shown in Figure 1,[13] the crucible with a coal sample is

Received: January 28, 2014
Revised: March 31, 2014
Published: April 1, 2014

   dx.doi.org/10.1021/ef500251h | *Energy Fuels* 2014, 28, 2993−3001

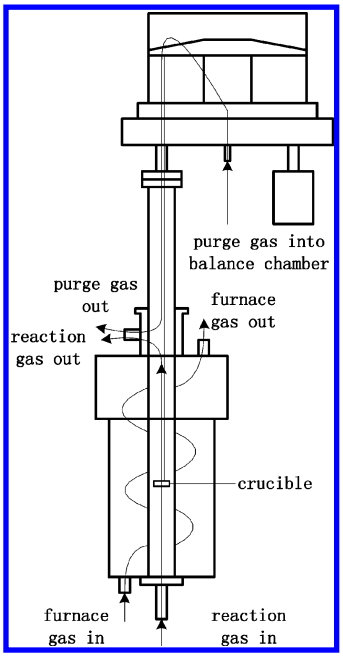

Figure 1. Schematic diagram of the P-TGA.

hung in the center of the furnace, where the hydropyrolysis takes place. Three gas streams, including the purge gas (He), the furnace gas (He), and the reaction gas (H_2), are injected from the high-pressure vessels into the P-TGA. The flow rates of gases are detected by the gas flow-meter and controlled by the valves. The purge gas is used to keep the pressure of the balance chamber and prevent the high-temperature reaction gas from entering the balance chamber; the furnace gas is used to balance the pressure in the reactor; and the reaction gas is used to react with the coal sample.

A bituminous coal sample is used in the experiments. The proximate and ultimate analyses of the bituminous coal are listed in Table 1. The coal sample is dried to remove moisture before CHP, so that the moisture volatilization process will not occur during the CHP process. About 14.5 mg of pre-dried coal is loaded in the crucible for each experiment. The temperature for the sample reaction is increased from the ambient value to 1000 °C with a ramping rate of 20 °C/min. The pyrolysis pressure is set as 0.1, 1, 2, 3, and 4 MPa, respectively. For each experiment, a blank sample experiment, in which the quartz sand is substituted for coal particles, is also implemented under the same conditions to compensate for the temperature drifts caused by the buoyancy.

3. RESULTS

3.1. Thermogravimetric Analysis. The comparison of TG and DTG curves under different pressures are shown in panels a and b of Figure 2, respectively. From those panels, the reaction kinetic characteristic parameters, including the initial pyrolysis temperature T_s, the maximum weight loss rate r_{max} and corresponding temperature T_{max}, and the mean weight loss rate r_{mean}, can be determined, as shown in Table 2. Thereinto, r_{mean} is calculated as the ratio of total weight loss to the reaction time during the experiment. Because only ash will be left when the coal is totally converted in the hydrogen atmosphere, the final weight loss V_∞ for all of the cases is then considered to be the mass of volatile and fixed carbon in the dry base coal sample. A reaction difficulty index, I, defined by eq 1, is also shown in Table 2. It can be used to reflect the difficulty of the CHP and CHG reactions under different pressures

$$I = \frac{r_{max} r_{mean} V_\infty}{T_s T_{max} \Delta t_{1/2}} \quad (1)$$

where, $\Delta t_{1/2}$ is the time span when r/r_{max} equates to 0.5; namely, $\Delta t_{1/2}$ is the time-based half-peak width. It should be noted that, in some literature, the temperature instead of time is used to reflect the half-peak width.[13] Because the temperature is increased with a constant rate, when the temperature is lower than 1273 K, both the time-based half peak and the temperature-based half peak can properly reflect the half-peak width. In the present work, however, the temperature will be kept constant when it reaches 1273 K. In this case, the temperature-based half-peak width will be smaller than the actual half-peak width. However, for the time-based half peak, this will not be a problem because the reaction time is always increasing. Thus, to avoid the inadequacy of the temperature-based half-peak width, the reaction time is chosen to better reflect the half-peak width in this work.

It can be seen from Figure 2a that the mass of the coal sample decreases with the reaction time increment. At the beginning and end of the whole reaction processes, the TG curves slope gently, while in the middle of the processes, the TG curves slope sharply. Thus, the TG curves have a reversed S shape. This is due to the extraction of the volatile in coal and the hydrogasification of char. From Figure 2b, it can be seen that, with the pressure increment, the appearing time of the peak position is found delayed when the reaction pressure is lower than 2 MPa, while it is found moving forward when the reaction pressure is higher than 2 MPa. The peak value decreases sharply when the pressure increases from 0.1 to 1 MPa and then increases gradually with the increment of pressure when the pressure is higher than 1 MPa. This is because when the reaction pressure is not higher than 1 MPa, hydrogasification will not be apparent and increased pressure will restrain the yield of volatiles because of Le Chatelier's principle.[14] For the reactions whose gaseous products are more than the gaseous reactants, e.g., the decomposition of large molecules and the coal pyrolysis process, an increasing pressure is not beneficial according to Le Chatelier's principle, which indicates that the reactions tending to counteract the pressure increment will be promoted with the pressure increment. When the reaction pressure is higher than 1 MPa, the CHG will be promoted and the reaction rate and its peak value will be increased. It can also be seen, from Figure 2b, that the effect of the pressure on the maximum weight loss rate gradually weakens as the pressure increases from 1 to 4 MPa. Although the maximum weight loss rate increases with the pressure increment, the extent of the weight loss increment decreases with the increasing pressure. This is mainly because the reaction pressure can affect the activity of the char generated after pyrolysis, and many researchers have reported that the

Table 1. Analysis of Coal

proximate analysis				ultimate analysis				
$moisture_{ad}$	$volatile\ matter_d$	$fixed\ carbon_d$	ash_d	C_d	H_d	O_d	N_d	total sulfer
5.60	19.11	49.87	31.02	55.67	3.22	5.68	1.02	3.39

dx.doi.org/10.1021/ef500251h | Energy Fuels 2014, 28, 2993−3001

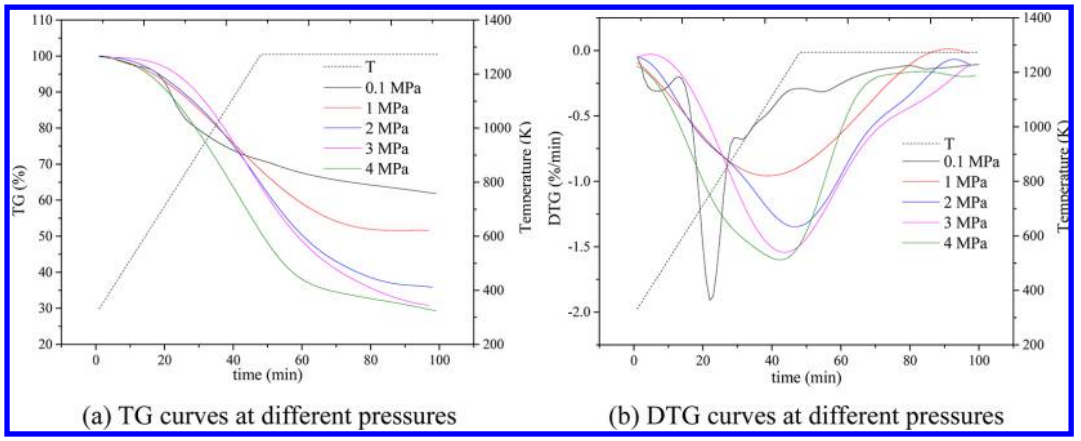

Figure 2. Thermogravimetric curves.

Table 2. Overall Reaction Characteristic Parameters of the Bituminous Coal in a Hydrogen Atmosphere

pressure (MPa)	T_s (°C)	T_{max} (°C)	r_{max} (%/min)	r_{mean} (%/min)	I (min^{-3} $°C^{-2}$)
0.1	133.9	464.3	−1.91	−0.38	1.0×10^{-6}
1	181.3	836.7	−0.96	−0.48	4.0×10^{-8}
2	225.3	998.1	−1.35	−0.64	5.8×10^{-8}
3	335.8	943.0	−1.54	−0.69	5.9×10^{-8}
4	192.2	911.3	−1.60	−0.70	1.1×10^{-7}

char activity will be decreased with the increase of the pyrolysis pressure.[15−17]

The initial pyrolysis temperature, T_s in Table 2, is found increasing with the increment of the reaction pressure when it is lower than 3 MPa, but the initial pyrolysis temperature will be decreased under the pressure of 4 MPa. This is mainly because, for the bituminous coal used in this work, when the pyrolysis pressure is not high (0.1−3 MPa), the inhibit effect of the pressure increment on the pyrolysis extraction will dominate and the initial pyrolysis temperature will be increased. When the pressure is higher than 3 MPa, because more hydrogen will enter the small and microsize pores in the coal structure, the combination of hydrogen with the heteroatoms (O, N, and S) and small free radicals will be enhanced under the higher pressure and this is beneficial to the extraction of the volatile. Thus, when the reaction pressure is 4 MPa, the initial pyrolysis temperature will be decreased. The maximum weight loss rate temperature, T_{max}, increases with the pressure increment when the pressure is lower than 2 MPa and then begins to decrease with the reaction pressure when the pressure becomes higher. The maximum weight loss rate decreases when the reaction pressure is increased from 0.1 to 1 MPa and then increases with the pressure increment. The reason is that, when the pressure is not higher than 1 MPa, the hydropyrolysis process will dominate and an increasing pressure will restrain the yield of the volatile. When the reaction pressure is higher than 1 MPa, hydrogasification will be promoted and the maximum weight loss rate will gradually increase with the pressure increment. Moreover, the mean weight loss rate is found increasing with the pressure increment. This is because the volatile only takes up a small fraction in the bituminous coal. When the reaction pressure is higher than 1 MPa, the hydrogasification process will be the main contributor to the weight loss. Thus, increasing the reaction pressure can increase the mean weight loss rate. The index, I, is also found decreasing with the pressure increasing from 0.1 to 1 MPa, and then it will gradually increase with the pressure increment, which indicates that the reaction process will be restrained when the pressure increases from 0.1 to 1 MPa, while it will be promoted when the pressure increases from 1 to 4 MPa. The reason is the same as that for the change trend of r_{max} mentioned above.

3.2. Kinetic Analysis. *3.2.1. Analysis Method.* It is known that hydrogen is not inert but can react with char and other species during the whole reaction process. In addition, volatile is only a small part in the bituminous coal. Thus, the contribution of hydrogasification to the total weight loss is obvious. Some researchers have studied both the pyrolysis and gasification processes when coal or biomass is chemically converted in the active atmosphere, such as H_2O and CO_2.[18,19] Because the pyrolysis process will take place at low temperatures and is much faster than the gasification process, char gasification is usually considered to follow the pyrolysis process. In the literature,[18] a specific temperature, such as 800 °C, was directly chosen as the critical point to distinguish the pyrolysis and gasification processes. For different reaction conditions, however, the critical temperature between the pyrolysis and gasification cannot be a determined value. In this work, 5−95% weight loss of the volatile contained in the coal sample is considered to be the major hydropyrolysis process, as reported in the literature,[11] and the following weight loss is considered to be caused by hydrogasification. Choosing 5−95% weight loss of the volatile as the main pyrolysis process can avoid the effects of unstable factors in the initial and final stages of the pyrolysis process. For example, at the beginning of the pyrolysis, the extraction of the residual moisture may affect the weight loss of the coal sample. At the end of the pyrolysis process, coal gasification will become important and may contribute to the weight loss of the coal sample. The kinetic equation for the CHP can be written as eq 2[20,21]

$$\frac{d\alpha}{dt} = kf(\alpha) = Ae^{-E/RT}f(\alpha) \quad (2)$$

where α is the conversion rate and can be calculated with eq 3, t is the pyrolysis time, k is the reaction rate constant and is calculated with the Arrhenius correlation, A is the pre-exponential factor, E is the activation energy, R is the universal gas constant, T is the reaction temperature, and $f(\alpha)$ is the kinetic mechanism function

$$\alpha = \frac{w_0 - w}{w_0 - w_\infty} \quad (3)$$

dx.doi.org/10.1021/ef500251h | Energy Fuels 2014, 28, 2993−3001

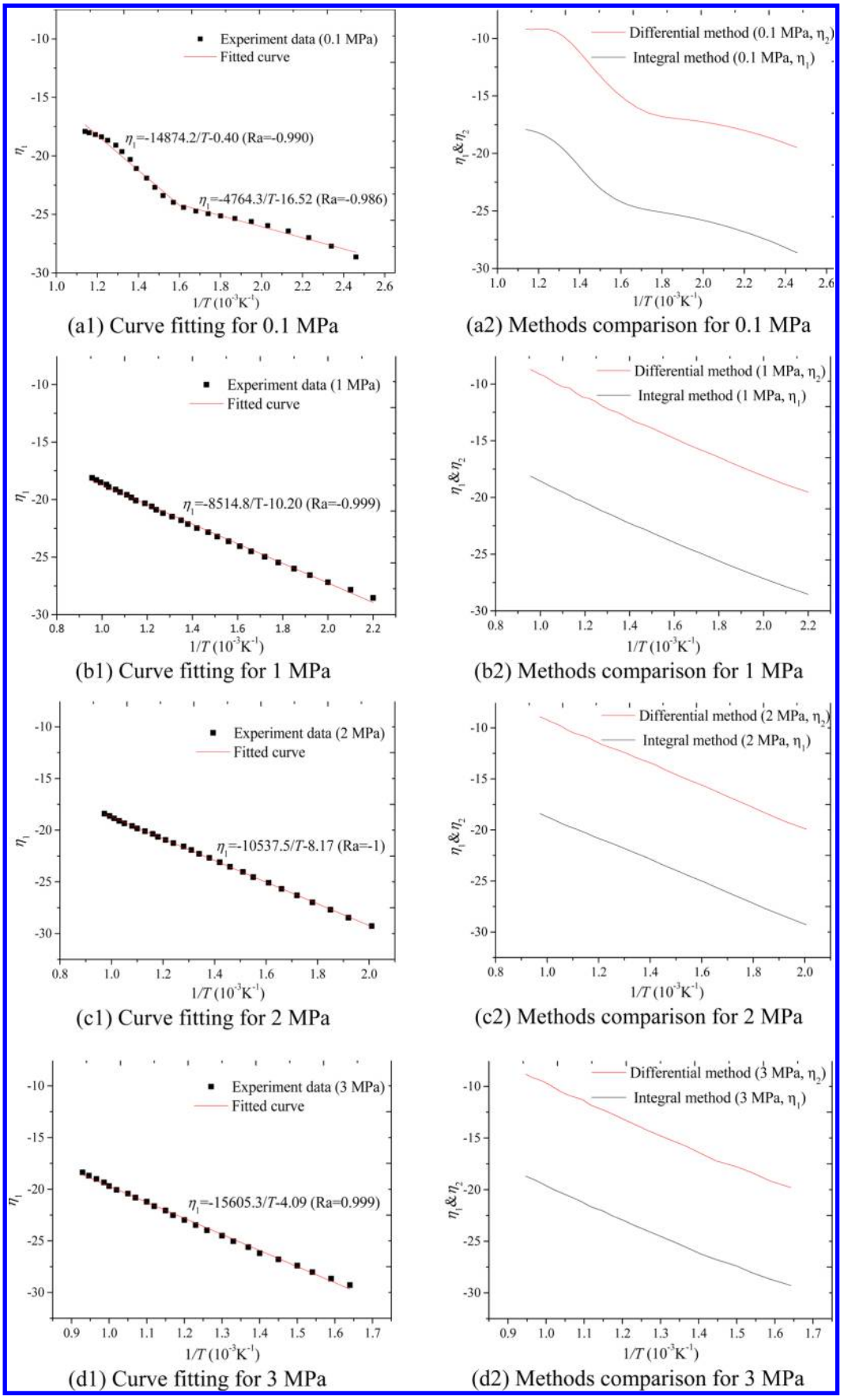

Figure 3. continued

dx.doi.org/10.1021/ef500251h | *Energy Fuels* 2014, 28, 2993−3001

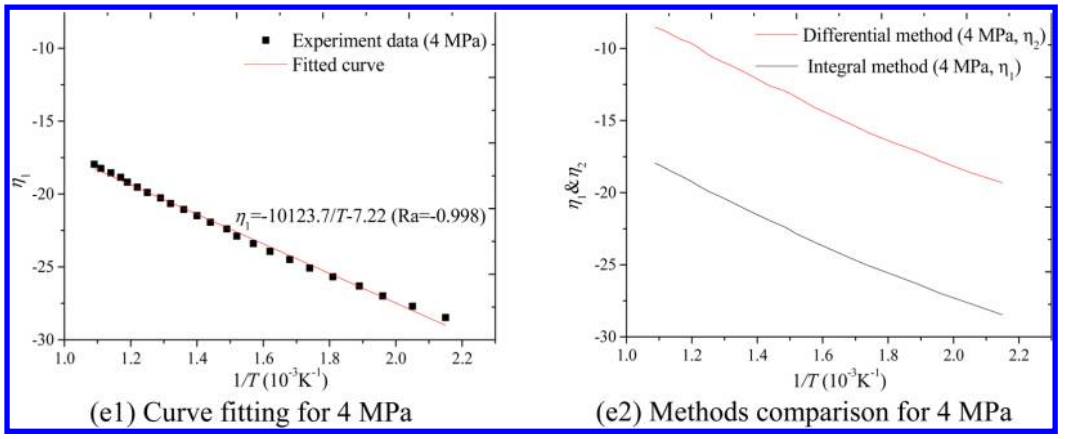

Figure 3. Curve fitting and method comparison for CHP.

where w_0 is the initial mass, w is the mass of the coal sample at any time during the whole reaction process, and w_∞ is the ash mass left in the end. Because E/RT is a much larger than unit in the common reaction temperature range, the Coats−Redfern approximation formula[22] is used and the kinetic correlation can finally be written as eq 4

$$\ln\left[\frac{G(\alpha)}{T^2}\right] = -\left(\frac{E}{RT}\right) + \ln\left(\frac{AR}{\beta E}\right) \tag{4}$$

where $G(\alpha)$ is the integral form of $f(\alpha)$ and β is the temperature ramping rate.

To find the proper kinetic mechanism function, the integral−differential method is used in this work.[23] The kinetic equation, eq 2, can be deducted to the corresponding differential form shown by eq 5 with the Achar−Brindley−Sharp−Wendworth method.[24,25]

$$\ln\left[\frac{\mathrm{d}\alpha}{f(\alpha)\mathrm{d}T}\right] = -\left(\frac{E}{RT}\right) + \ln\left(\frac{A}{\beta}\right) \tag{5}$$

The common mechanism functions reported in the literature[26] are investigated, and finally, the random nucleation and later growth mechanism function with the exponent, m, of 4 developed by Avrami[27−29] is found to have the best performance. Thus, this mechanism function is chosen to describe the CHP process. The mechanism function and the corresponding integral form are written as eqs 6 and 7.

$$f(\alpha) = \frac{1}{m}(1-\alpha)[-\ln(1-\alpha)]^{(1-m)} \tag{6}$$

$$G(\alpha) = [-\ln(1-\alpha)]^m \tag{7}$$

For the CHG process, because the reaction of char and H_2 must be considered, the kinetic equation should be written as eq 8[18,30]

$$\frac{\mathrm{d}\alpha}{\mathrm{d}t} = Kf(\alpha) = A\mathrm{e}^{-E/RT}f(\alpha)p_{\mathrm{H_2}}^n \tag{8}$$

where $p_{\mathrm{H_2}}^n$ is the hydrogen partial pressure and n denotes the reaction order. Because the whole reaction process takes place in almost a pure H_2 atmosphere, the reaction pressure is then the hydrogen pressure. Also, because the amount of hydrogen is considerably larger than that of the coal sample, for a specific experiment condition, the hydrogen pressure can be considered as constant. Because, for a specific experiment condition, the pre-exponent factor A is a constant value, the terms of hydrogen pressure $p_{\mathrm{H_2}}^n$ and pre-exponent factor A in eq 8 can then be combined into a new pre-exponent factor A^*. Then, eq 8 can be rewritten as eq 9 and the following correlation, which is similar to eq 2.

$$\frac{\mathrm{d}\alpha}{\mathrm{d}t} = Kf(\alpha) = A^*\mathrm{e}^{-E/RT}f(\alpha) \tag{9}$$

Some researchers once directly used the shrinking core model[18] as the kinetic mechanism function for the gasification process. However, in this work, it is found that the random nucleation and later growth mechanism shows better performance in the CHP and CHG processes. Thus, this mechanism rather than the shrinking core model is chosen as the kinetic mechanism function for the CHG process.

3.2.2. Calculation Results. On the basis of eq 4, the plots of $\ln[G(\alpha)/T^2]$ versus $1/T$ and the corresponding fitted curves for the CHP process are shown in panels a1−e1 of Figure 3. The comparisons of the curves obtained from the integral method (eq 4) and the differential method (eq 5) are shown in panels a2−e2 of Figure 3. The plots of $\ln[G(\alpha)/T^2]$ versus $1/T$ and the corresponding fitted curves for the CHG process are shown in panels a1−e1 of Figure 4. The comparisons of the curves obtained from the integral and differential methods are shown in panels a2−e2 of Figure 4. The calculated Arrhenius kinetic results for both the CHP and CHG processes are listed in Tables 3 and 4, respectively. In the panels, η_1 is used to denote $\ln[G(\alpha)/T^2]$ in eq 4 for the integral method and η_2 is used to denote $\ln[\mathrm{d}\alpha/f(\alpha)\mathrm{d}T]$ for the differential method. As deducted elsewhere,[13] the slope of the curves obtained by the integral and differential methods reflect the term $-(E/RT)$ and the difference of the curves reflects $\ln(R/E)$.

From panels a1−e1 of Figure 3, it can be seen that the points generated with the random nucleation and later growth mechanism have good linearity because the regression coefficients are very close to unit. From panels a2−e2 of Figure 3, it can be seen that the curves obtained using the integral and differential methods are found basically parallel to each other, which indicates that the activation energies calculated from the differential and integral methods are very close to each other. All of these panels indicate that the random nucleation and later growth mechanism is proper to reflect the CHP kinetic process. From panels a1−e1 of Figure 4, it can be seen that the points generated with the RNLG mechanism have good linearity because all of the regression coefficients are very close to unit. From panels a2−e2 of Figure 4, it can be seen that

dx.doi.org/10.1021/ef500251h | Energy Fuels 2014, 28, 2993−3001

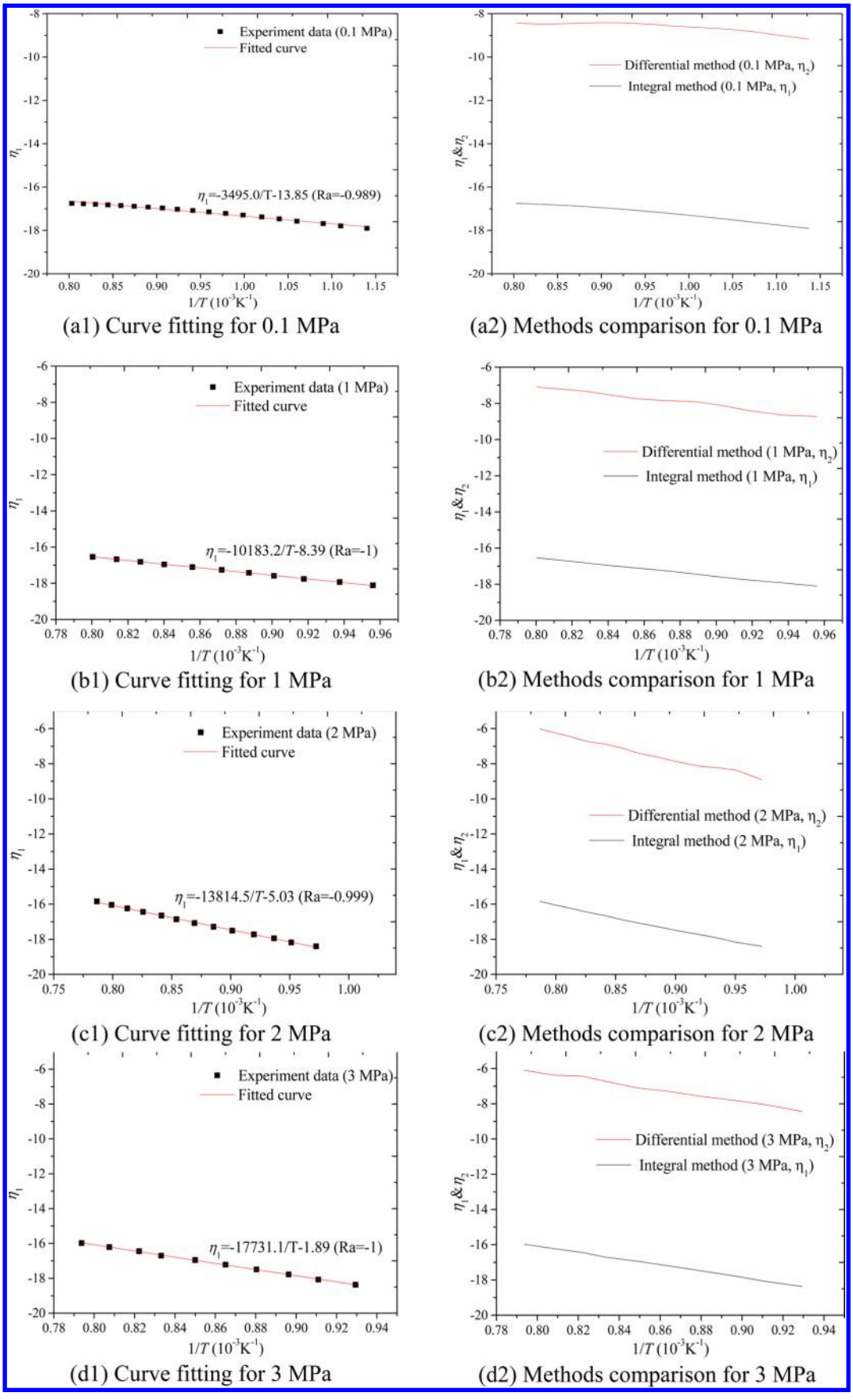

Figure 4. continued

dx.doi.org/10.1021/ef500251h | *Energy Fuels* 2014, 28, 2993−3001

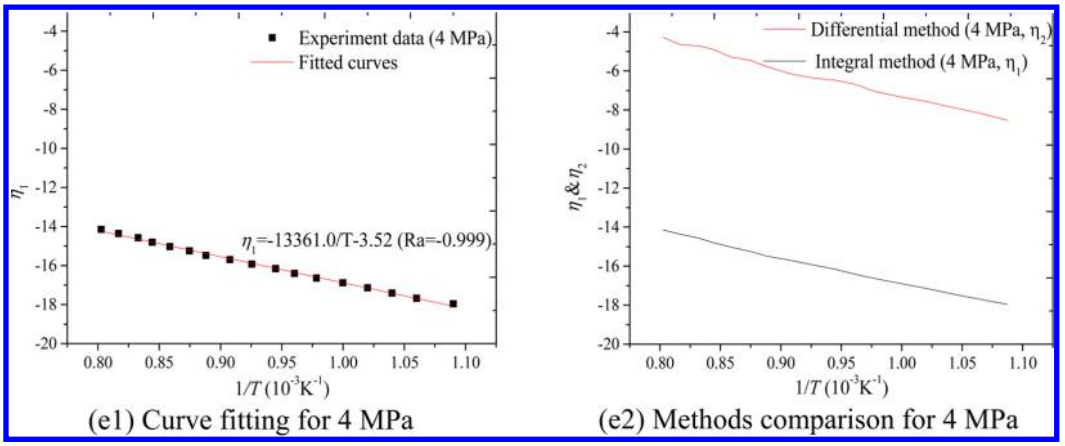

Figure 4. Curve fitting and method comparison for CHG.

Table 3. Kinetic Parameters for the CHP Process under Different Pressures

pressure (MPa)	temperature range (°C)	E (kJ/mol)	A (min^{-1})	$-R_a$	$\ln(R/E)$	D_{ave}
0.1	134−343	40.36	7.89×10^{-3}	0.986	−8.49	−8.69
	343−606	119.65	1.04×10^{5}	0.990	−9.57	−9.45
1	181−773	70.80	6.33×10^{0}	0.999	−9.05	−9.24
2	225−755	87.61	5.96×10^{1}	1	−9.26	−9.40
3	336−803	88.60	9.03×10^{1}	0.999	−9.27	−9.77
4	192−646	84.17	1.48×10^{2}	0.998	−9.22	−9.37

Table 4. Kinetic Parameters for the CHG Process under Different Pressures

pressure (MPa)	temperature range (°C)	E (kJ/mol)	A (min^{-1})	$-R_a$	$\ln(R/E)$	D_{ave}
0.1	606−972	290.59	6.76×10^{-2}	0.989	−8.16	−8.58
1	773−976	84.67	4.61×10^{1}	1	−9.23	−9.42
2	755−998	114.86	1.81×10^{3}	0.999	−9.53	−9.71
3	803−987	152.68	9.60×10^{4}	1	−9.81	−9.92
4	646−973	111.09	7.92×10^{2}	0.999	−9.50	−9.67

the curves obtained using the integral and differential methods are found basically parallel to each other, which indicates that the values of the activation energy obtained from the differential and integral methods are very close. All of these figures indicate that the random nucleation and later growth mechanism is proper to reflect the CHG kinetic process.

D_{ave} in Tables 3 and 4 is the average of $\eta_1-\eta_2$ in the corresponding temperature range. If the pre-exponential factor A calculated from the integral and differential methods, is close to each other, the average value of D_{ave} should be close to the calculated value, $\ln(R/E)$. From the comparisons of the two values in Tables 3 and 4, they are found agreeing with each other very well, which indicates that the random nucleation and later growth mechanism can properly reflect both the CHP and CHG processes.

3.2.3. KCE. The KCE between the activation energy E and the pre-exponential factor A can be detected in many kinetic processes. For the kinetic processes having KCE, the Arrhenius parameters E and A will exhibit the following relationship as shown by eq 10:[31]

$$\ln A = aE + b \tag{10}$$

where a and b are constants for a series of related kinetic processes. Equation 10 indicates that, if the kinetic processes obey the KCE, $\ln A$ and E will present a linear relationship. Using this relationship, the kinetic parameters under different conditions can be correlated. It can be used to predict the Arrhenius parameters when limited data is available. Taking the logarithm for both sides of the Arrhenius equation, eq 11 can be obtained.

$$\ln k = \ln A - \frac{E}{RT} \tag{11}$$

When eqs 10 and 11 are combined, eq 12 can be obtained.

$$\ln k = b + \left(a - \frac{1}{RT}\right)E \tag{12}$$

From eq 12, it can be found that there will be a temperature point T^* that makes $1/RT^*$ equal to a. At this temperature, $\ln k^*$ will equal b. At this point, eq 10 can then be rewritten as eq 13.

$$\ln A = \frac{1}{RT^*}E + \ln k^* \tag{13}$$

Thus, for all of the related kinetic processes during which KCE exists, there will be a temperature point at which these processes have the same kinetic constant. In addition, if $\ln k$ is plotted against $1/T$ for these processes, all of the straight lines should intersect at one point, which is the so-called the isokinetic point.

In this section, the KCE during the CHP and CHG processes are investigated, respectively. The plot of $\ln A$ versus E for the CHP process is depicted in Figure 5, and that for the CHG process is depicted in Figure 6.

dx.doi.org/10.1021/ef500251h | *Energy Fuels* 2014, 28, 2993−3001

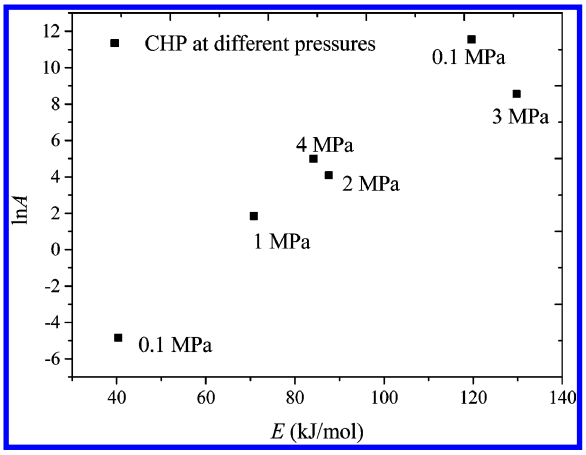

Figure 5. ln A versus E for the CHP.

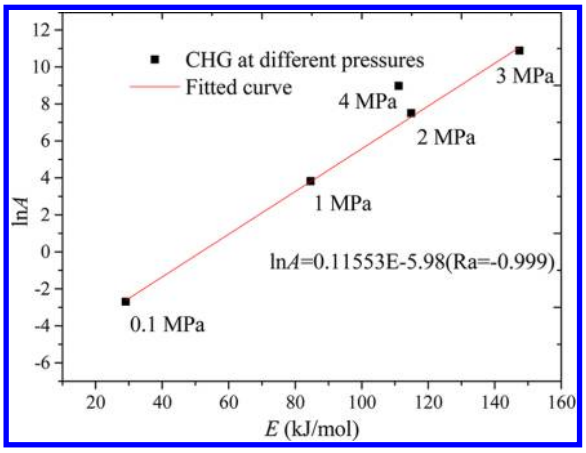

Figure 6. ln A versus E for the CHG.

From Figure 5, it can be seen that the points do not present a good linear relationship for the CHP processes at different pressures. However, for the CHG processes, as depicted in Figure 6, the points exhibit good linearity, except for the point at 4 MPa. Thus, it is concluded from Figures 5 and 6 that KCE does not exist for the CHP process when the reaction pressure ranges from 0.1 to 4 MPa. When the pressure ranges from 0.1 to 3 MPa, KCE can be detected for the CHG process. From the analyses above, it is known that, when the processes have KCE, an isokinetic point can be found for these processes and the plots of ln k versus $1/T$ will intersect at this point. The plot of ln k against $1/T$ for the CHG processes when the pressure is lower than 3 MPa is shown in Figure 7.

From Figure 7, it can be seen that the straight lines converge at one point around 0.001. From Figure 6, it is known that the parameter a in eq 10 is 0.115 53. Thus, from eq 12, it is known that the temperature should be $1/(0.11553R) = 1041.0$ K. Therefore, it is believed that the CHG processes have the KCE when the pressure is within 3 MPa and the isokinetic point is at the temperature of 1041.0 K. The isokinetic point here means that, when the temperature is 1041.0 K, all of the CHG processes at different pressures will have the same kinetic constant, k, and the value is calculated as 2.529×10^{-3} min^{-1}.

4. CONCLUSION

To find out the detailed kinetic process, both the CHP and CHG kinetic characteristics are analyzed with a P-TGA in this work. A series of TG and DTG curves of the whole reaction processes at different reaction pressures are obtained and compared. The changing trend of the important parameters, such as the initial pyrolysis temperature, the weight loss peak rate and corresponding temperature, the average weight loss rate, and the reaction difficulty index, are analyzed first. Then, the kinetic triplets for the CHP and CHG processes at different pressures are defined and calculated. Finally, the kinetic compensation effect in the CHP and CHG processes are investigated, and the isokinetic points of the processes are detected. After this work, meaningful conclusions are obtained and can be drawn as follows: (1) The weight loss peak value decreases sharply when the pressure increases from 0.1 to 1 MPa. Then, when the reaction pressure increases from 1 to 4 MPa, it gradually increases but the increment extent decreases. (2) The reaction difficulty index decreases when the reaction pressure increases from 0.1 to 1 MPa and then begin to increase when the pressure is increased from 1 to 4 MPa. This indicates that the reaction process will be restrained when the pressure increases from 0.1 to 1 MPa, while it will be promoted when the pressure increases from 1 to 4 MPa. (3) The random nucleation and later growth kinetic mechanism function with the exponent of 4 is found proper for both the CHP and CHG processes. (4) The KCE cannot be detected during the CHP process. When the pressure is within 3 MPa, KCE can be detected for the CHG process and the isokinetic point is found at the temperature of 1041.0 K.

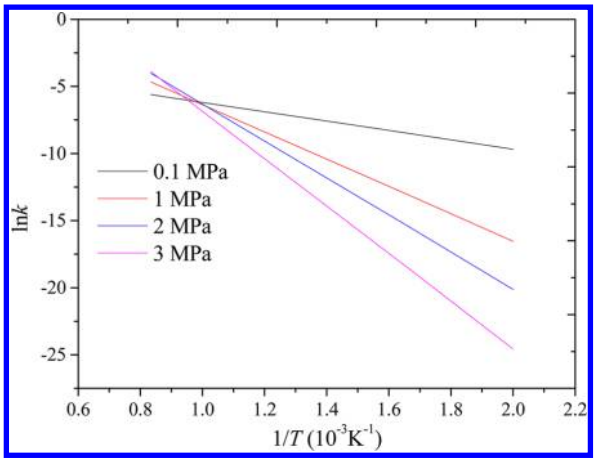

Figure 7. Isokinetic point of the CHG processes.

AUTHOR INFORMATION

Corresponding Author

*Telephone: +86-10-5168-8542. Fax: +86-10-5168-8404. E-mail: hebs@bjtu.edu.cn.

Notes

The authors declare no competing financial interest.

ACKNOWLEDGMENTS

The authors gratefully acknowledge financial support from the National Natural Science Foundation of China (NSFC, 50876008 and 51176009) for this work.

REFERENCES

(1) Steinberg M. *Process for Conversion of Coal to Substitute Natural Gas (SNG)*; HCE, LLC: Oakton, VA, Aug 2005; Contract HCEI-8-05-001r2, http://www.hceco.com/HCEI805001.pdf.

(2) Yan, L. B.; He, B. S.; Pei, X. H.; Li, X. S.; Wang, C. J.; Liang, H. X. Kinetic model and prediction for coal hydrogasification. *Int. J. Hydrogen Energy* **2013**, *38*, 4513−4523.
(3) Yan, L. B.; He, B. S.; Pei, X. H.; Wang, C. J.; Li, X. S.; Duan, Z. P. Kinetic models for coal hydrogasification and analyses of hydrogasification characteristics in entrained-flow gasifiers. *Energy Fuels* **2013**, *27*, 6388−6396.
(4) Yan, L. B.; He, B. S.; Pei, X. H.; Wang, C. J.; Liang, H. X.; Duan, Z. P. Computational fluid dynamics based evaluation and optimization of an entrained-flow gasifier potential for coal hydrogasification. *Energy Fuels* **2013**, *27*, 6397−6407.
(5) Tang, L. H.; Zhu, Z. B.; Gu, H. X.; Zhang, C. F. The effect of coal rank on flash hydropyrolysis of Chinese coal. *Fuel Process. Technol.* **1999**, *60*, 195−202.
(6) Porada, S. A. Comparison of basket willow and coal hydrogasification and pyrolysis. *Fuel Process. Technol.* **2009**, *90*, 717−721.
(7) Zhang, A.; Kaiho, M.; Yasuda, H.; Zabat, M.; Nakano, K.; Yamada, O. Fundamental studies on hydrogasification of Taiheiyou coal. *Energy* **2005**, *30*, 2243−2250.
(8) Falk, A. Y.; Schuman, M. D.; Kahn, D. R. *Advancement of Flash Hydrogasification: Task VIII Performance Testing*; Morgantown Energy Technology Center: Morgantown, WV, 1986; Contract DEAC21-78ET10328, http://www.osti.gov/bridge/purl.cover.jsp?purl=/5377768-SKAxm4/5377768.pdf.
(9) Friedman, J. *Development of a Single-Stage, Entrained-Flow, Short-Residence-Time Hydrogasifier*; National Technical Information Service: Alexandria, VA, 1979; Contract FE-2518-24.
(10) Epstein, M.; Chen, T. P.; Ghaly, M. A. *An Analysis of Coal Hydrogasification Process*; Energy Research and Development Administration: Washington, D.C., 1977; Contract EF-77-A-01-2565, www.osti.gov/bridge/servlets/purl/6074682-KtEPFx/6074682.pdf.
(11) Zhou, L. M.; Jia, Y. Y.; Nguyen, T. H.; Adesina, A. A.; Liu, Z. R. Hydropyrolysis characteristics and kinetics of potassium-impregnated pine wood. *Fuel Process. Technol.* **2013**, *116*, 149−157.
(12) Xu, W. C.; Kumagai, M. Sulfur transformation during rapid hydropyrolysis of coal under high pressure by using a continuous free fall pyrolyzer. *Fuel* **2003**, *82*, 245−254.
(13) Yan, L. B.; He, B. S.; Hao, T. Y.; Pei, X. H.; Li, X. S.; Wang, C. J.; Duan, Z. P. Thermogravimetric study on the pressurized hydropyrolysis kinetics of a lignite coal. *Int. J. Hydrogen Energy* **2014**, DOI: 10.1016/j.ijhydene.2014.03.060.
(14) George, W. R. *Chemical Reactions and Chemical Reactors*; John Wiley and Sons, Inc.: Hoboken, NJ, 2009.
(15) Gadiou, R.; Bouzidi, Y.; Prado, G. The devolatilisation of millimetre sized coal particles at high heating rate: The influence of pressure on the structure and reactivity of the char. *Fuel* **2002**, *81*, 2121−2130.
(16) Yang, H. P.; Chen, H. P.; Ju, F. D.; Wang, J.; Zhang, S. H. Study on pressurized pyrolysis and gasification of Chinese typical coal samples. *Proc. CSEE* **2007**, *27*, 18−22 (in Chinese).
(17) Messenböck, P. C.; Paterson, N. P.; Dugwell, D. R.; Kandiyoti, R. Factors governing reactivity in low temperature coal gasification. Part 1. An attempt to correlate results from a suite of coals with experiments on maceral concentrates. *Fuel* **2000**, *79*, 109−121.
(18) Xiao, J.; Shen, L. H.; Deng, X.; Wang, Z. N.; Zhong, X. L. Thermogravimetric study on catalytic pyrolysis gasification of biomass. *Acta Energ. Sol. Sin.* **2009**, *30*, 1252−1257 (in Chinese).
(19) İffet, Y. E.; Sabriye, P.; Hale, S. Pyrolysis kinetics of Turkish bituminous coals by thermal analysis. *Turk. J. Eng. Environ. Sci.* **2004**, *28*, 233−239.
(20) Jankovi, B. Kinetic analysis of the nonisothermal decomposition of potassium metabisulfite using the model-fitting and isoconversional (model-free) methods. *Chem. Eng. J.* **2008**, *139*, 128−135.
(21) Carrasco, F.; Gámez-Pérez, J.; Santana, O. O.; Maspoch, M. L. Processing of poly (lactic acid)/organo-montmorillonite nanocomposites: Microstructure, thermal stability and kinetics of the thermal decomposition. *Chem. Eng. J.* **2011**, *178*, 451−460.
(22) Coats, A. W.; Redfern, J. P. Kinetic parameters from thermogravimetric data. *Nature* **1964**, *201*, 68−69.
(23) Zhang, C. Q.; Wei, L. H.; Ren, G. P.; Jiang, X. M. Research on pyrolysis characteristics and mechanism of micro-pulverized and common-pulverized coal. *J. Harbin Inst. Technol.* **2006**, *38*, 1948−1951 (in Chinese).
(24) Achar, B. N. N.; Bridley, G. W.; Sharp, J. H. Thermal decomposition kinectics of some new unsaturated polyesters. *Proc. Int. Clay. Conf.* **1966**, *1*, 67−73.
(25) Sharp, J. H.; Wentworth, S. A. Kinetic analysis of thermogravimetric data. *Anal. Chem.* **1969**, *41*, 2060−2062.
(26) Hu, R. Z.; Shi, Q. Z. *Thermal Analysis Kinetics*; Sciences Press: Beijing, China, 2001 (in Chinese).
(27) Avrami, M. Kinetics of phase change. I General theory. *J. Chem. Phys.* **1939**, *7*, 1103−1112.
(28) Avrami, M. Kinetics of phase change. II Transformation-time relations for random distribution of nuclei. *J. Chem. Phys.* **1940**, *8*, 212−224.
(29) Avrami, M. Granulation, phase change, and microstructure kinetics of phase change. III. *J. Chem. Phys.* **1941**, *9*, 177−184.
(30) Song, H.; Shah, K.; Doroodchi, E.; Wall, T.; Moghtaderi, B. Analysis on chemical reaction kinetics of CuO/SiO_2 oxygen carriers for chemical looping air separation. *Energy Fuels* **2014**, *28* (1), 173−182.
(31) Liu, N. A.; Wang, B. H.; Fan, W. C. Kinetic compensation effect in biomass thermal decomposition. *Fire Saf. Sci.* **2002**, *11*, 63−69 (in Chinese).